DOI: 10.61782/fa.2023.0343

forum acusticum 2023

ACOUSTIC BLACK HOLE EFFECT IN DUCTED GEOMETRIES FOR ENHANCED DISSIPATION AT LOW FREQUENCIES

Teresa Bravo[1*] **Cedric Maury**[2]
[1] Spanish National Research Council (CSIC), Madrid, Spain
[2] Aix Marseille Univ, CNRS, Centrale Marseille, Marseille, France

ABSTRACT[*]

Improvement of acoustic absorption and transmission in the low frequency range when facing constraints on total volume and weight constitutes a constant challenge in the field of noise control. Emergence of acoustic metamaterials has allowed the development of compact sub-wavelength absorbers that can provide solutions in terms of the required wideband low-frequency sound dissipation. In a lined waveguide, the effective velocity of the incoming sound can be progressively reduced to zero leading to the Acoustic Black Hole (ABH) effect. In this work, this concept of sound trapping has been mostly explored for widely-opened ABH silencer for the reduction of the transmission properties without obstructing flow circulation. Attention has been paid to the attenuation of the acoustic back-reflections that can be of interest for improving engine combustion efficiency for instance. Parametric studies are carried out to study the influence of the physical ABH factors on the acoustic performance. We have also performed a causality-constrained optimization to determine the minimum bandwidth-to-length ratio required for a fixed dissipation requirement. Results have been validated with experimental results.

Keywords: *metasilencer, acoustic black hole, low frequency dissipation.*

[*]***Corresponding author***: *teresa.bravo@csic.es.*

1. INTRODUCTION

Improvement of acoustic absorption and sound insulation at low frequencies using structures with limited size or weight constitutes a long-standing engineering challenge in the field of environmental noise control. Porous and fibrous absorbers show good broadband performance in the high frequency range, but optimal solutions for low frequency problems are too bulky and not suitable to large-scale applications. Micro-Perforated Panels backed by a rigid cavity [1, 2] are sound absorbers that have proved to be efficient in this frequency range when properly selecting their physical constitutive parameters [3, 4]. In spite of this, the attenuation values are restricted within two or three octaves bandwidth around their Helmholtz-type resonance. The addition of serial or parallel arrays of rigidly-backed MPP resonators with different cavity depths or perforation ratios can broaden the bandwidth of interest by merging the multiple discrete narrowband resonances for each individual micro-perforated resonator [5, 6]. The drawback of this strategy is the trade-off that is normally required in real problems involving the maximum absorption value, the absorption bandwidth and the absorbent overall thickness [7, 8].

Development of acoustic metamaterials has allowed the growth of sub-wavelength absorbers that can provide solutions in terms of the required wideband low-frequency sound dissipation [9, 10]. Metamaterials derive their properties from their designed structures and geometries. Unlike traditional composites, acoustic metamaterials can exceed known bounds on conventional material properties. That is accomplished by exploiting subwavelength micro structure that has been fabricated from ordinary materials and embedded in a background medium (for air- or waterborne acoustic waves, the background medium is simply the surrounding fluid). The novel effective properties of acoustic metamaterials enable to manipulate

acoustic wave fields in ways that are impossible to achieve with naturally occurring materials or traditional composite structures. The response of properly defined unit cells can be translated into averaged effective parameters, namely an effective density and bulk modulus [11, 12]. For instance, the introduction of periodic resonant inclusions induce negative effective properties that create "stop-bands" where sound transmision is forbidden.

Tunable resonance systems can be conceived to design selective dissipation filters for the propagation of sound waves in a lined waveguide. The behavior of acoustic waves in the presence of a resonant metamaterial in a ducted system can be affected by the slow sound generation [13]. The goal is then the reduction of the incoming sound wave velocity resulting in a non-reflecting edge condition [14] with the sound waves, eventually confined in the meta-structure. It has been coined as an Acoustic Black Hole (ABH) and presents great potential for acoustic energy trapping.

This technique has been originally developed for passive vibration control. Vibrational black holes are made up of suitably sharpened beams or plate edges that slow down and prevent reflection of flexural waves at their boundaries [15]. A practical realization has been performed using a series of rigid discs fixed on a rod inside a tube with varying diameters according to a parabolic law. Energy absorption can be enhanced in areas of low velocity by the insertion of absorbing materials. ABHs constitute also retarding structures induced by a power law decay of the wave velocity, but with a different propagation operator [16]. Guasch et al. [17] studied the ABH effect using the transfer matrix method to predict the absorption performance of linear and quadratic ABH duct terminations as well as the influence of their physical parameters. It was found that this solution tends to the wave solution in a metafluid with power-law varying density using a high number of rings.

The ABH concept has also been considered for open-ended waveguides, in which the reduction of both absorption and transmission inside the metamaterial has to be accomplished. This configuration has been shown to be efficient provided that the ratio between the inlet and outlet radii stays greater than 10 [14]. Further investigations have been carried out analyzing the sensitivity of ABHs to truncation effects, the different damping mechanisms and the power-law decay rate that has to be selected to maximize the dissipation mechanisms. Zhang and Cheng [18] add damping by introducing micro-perforated boundaries that considerably improved the broadband low-frequency performance of open-ended ABHs. They proved that the truncation length at the extremity increased the cut-off frequency for the effective absorption range.

Concerning widely-opened mufflers, the transfer matrix method has also been used for performance predictions and the results have been experimentally validated on 3D printed prototypes for the no-flow case, with an inlet/outlet radius ratio equal to 2 [19]. Current trends are paying attention to the presence of a mean flow with the development of metamaterial windows [20] to allow both noise control and natural ventilation. The same considerations have been taken into account for the development of ultra-sparse acoustic ventilated meta-barriers [21]. Sound insulation and airflow transport have been experimentally demonstrated with a measured wind velocity ratio staggeringly higher than 90%.

In the present work, we aim at determining from optimization studies the main parameters of ABH duct liners that limit their low frequency broadband performance under a range of environmental conditions. We will focus on the design of a compact fully-opened ABH to get both low reflection and transmission without duct section variation and in the no-flow case. Special attention will be paid to the causal-based limitation performance of the metamuffler for optimal dissipation in the low frequency range. This subject has been studied before within the frame of rigidly-backed microperforated partitions [7, 8] and will be extended here to the case of open-ended configurations. Section 2 will present the model of the ABH duct liner analyzing in detail the reduction in the velocity of the incident sound wave. Section 3 will present parametric studies on the ABH acoustic performance whose causal-based optimization will be discussed in Section 4 and experimentally verified in Section 5. The main conclusions and guidelines for future work will be outlined in Section 6.

2. THEORETICAL MODEL

2.1 Reduction of the wave velocity

The ABH duct system that is proposed in this work is outlined in Figure 1. It is composed of set of ring sections separated by air cavities and distributed over an overall length L along the axial dimension. The radii of the air cavities in the fully-opened silencer progressively increase from 0 to R following a power law, and it is expanding from the inlet situated at $z=-L$ towards the outlet at $z=0$.

The analytical expressions that govern the wave propagation into the retarding structure have been defined in [15]. Taking the convention $e^{j\omega t}$, the linearized mass conservation equation in a ducted geometry with a wall

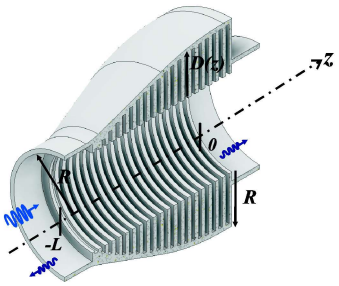

Figure 1. Schema of the ABH fully-opened configuration.

impedance on the boundary varying along the duct axis is given by [15]

$$\frac{\partial v_z}{\partial z}+\frac{v_n}{r_H}+\frac{\mathrm{d}(\log S)}{\mathrm{d}z}v_z=-\frac{\mathrm{j}\omega}{\rho_0 c_0^2}p,\quad -L<z<0\ , \qquad (1)$$

with v_z the axial velocity component, $v_n=p/Z$ the normal velocity over the boundary $\Sigma(r=R,-L<z<0)$ and p the acoustic pressure. $r_H=S/U$ is the hydraulic radius with S the cross-sectional area of the duct and U the circumference of the lining.

Introducing the linearized momentum conservation equation, $-\mathrm{j}\omega\rho_0 v_z=\partial p/\partial z$ into Eq. (1) and taking into account that $\mathrm{d}(\log S)/\mathrm{d}z=0$ for a fully-opened muffler with constant section, a plane wave equation is provided as

$$\frac{\mathrm{d}^2 p}{\mathrm{d}z^2}+k_0^2\left[1-\mathrm{j}\frac{y(z)}{k_0 r_H}\right]p=0\ , \qquad (2)$$

where $k_0=\omega/c_0$ is the acoustic wavenumber and $y=Z_0/Z$ is the wall specific admittance normalised by $Z_0=\rho_0 c_0$ the fluid characteristic impedance with ρ_0 the air density and c_0 the sound speed. The wall admittance of the ABH constituted of a continuous distribution of annular cavities can be approximated in the low frequency range ($k_0R<<1$), by

$$y(z)=\mathrm{j}k_0\left[R^2-(R+D(z))^2\right]\ . \qquad (3)$$

When introducing this expression into Eq. (2), one obtains

$$\frac{\mathrm{d}^2 p}{\mathrm{d}z^2}+k_0^2\left[1+\frac{2}{R}\left(D(z)+\frac{D^2(z)}{2R}\right)\right]p=0\,, \qquad (4)$$

that can be reduced to a Helmholtz equation when the cavity depths increases with the law $D(z)=R(1-\varphi_m(z))$, with $\varphi_m(z)=(-z)^m/L^m$, $m>0$. With this assumption, the wavenumber of the acoustic wave propagating inside the ABH silencer takes the expression $k_z(z)=k_0(2-\varphi_m(z))$, and the corresponding phase speed is given by

$$c_z(z)=\frac{c_0}{2-\varphi_m(z)}\ . \qquad (5)$$

It can be noted that the acoustic wave phase speed decreases progressively from c_0 at the inlet towards $c_0/2$ at the ABH outlet. This situation is clearly different from the closed ABHs where the phase and group velocity decrease to zero when approaching the ABH termination [17].

2.2 Transfer Matrix Formulation

An analytical description is developed using the Transfer Matrix Method (TMM) for a widely-open ABH constituted of a finite number of annular cavities and parameterized in discrete form as $D_i=R(1-\varphi_m(z_i))$ with $i=1,...,N$ and $m>0$. Assuming plane wave propagation in the duct and the adjacent cavities, they are represented by the localized sidebranch volume admittance $Y_{\mathrm{cav},i}=S_{\mathrm{cav}}y(z_i)/Z_0$, with $y(z_i)$ given by Eq. (3) and $S_{\mathrm{cav}}=2\pi Rd$ the cavities entrance area. Applying continuity of the acoustic pressure and acoustic flow rate across the i^{th} cavity-ring unit leads to the relationship, $[p_i\ u_i]^{\mathrm{T}}=\mathbf{T}_i[p_{i+1}\ u_{i+1}]^{\mathrm{T}}$, between the pressure and volume velocity fields at the input interface $[p_i\ u_i]^{\mathrm{T}}$ and those at the output interface $[p_{i+1}\ u_{i+1}]^{\mathrm{T}}$, with $\mathbf{T}_i$ the associated transfer matrix given by

$$\mathbf{T}_i=\begin{bmatrix}\cos(k_0 d) & \mathrm{j}\frac{Z_0}{S}\sin(k_0 d)\\ \mathrm{j}\frac{S}{Z_0}\sin(k_0 d) & \cos(k_0 d)\end{bmatrix}\cdot \begin{bmatrix}\cos(k_0 d_t) & \mathrm{j}\frac{Z_0}{S}\sin(k_0 d_t)\\ \mathrm{j}\frac{S}{Z_0}\sin(k_0 d_t) & \cos(k_0 d_t)\end{bmatrix}\begin{bmatrix}1 & 0\\ Y_{\mathrm{cav},i} & 1\end{bmatrix}\ . \qquad (6)$$

The overall transfer matrix $\mathbf{T}$ between inlet and outlet satisfies $[p_1\ u_1]^{\mathrm{T}}=\mathbf{T}[p_{N+1}\ u_{N+1}]^{\mathrm{T}}$ and is expressed as the product of the transfer matrices, $\mathbf{T}=\prod_{i=1}^{N}\mathbf{T}_i=\begin{bmatrix}T_{11} & T_{12}\\ T_{21} & T_{22}\end{bmatrix}$.

Assuming a perfect anechoic downstream condition, the pressure transmitted p_{N+1} is related to the volume velocity

u_{N+1} by $p_{N+1} = Z_0 u_{N+1}/S$. The solution for the reflection and transmission coefficients are given by

$$\begin{cases} r = \dfrac{(T_{11} + z_0 T_{12}) - (T_{21} + z_0 T_{22})}{(T_{11} + z_0 T_{12}) + (T_{21} + z_0 T_{22})} \\ t = \dfrac{1 + r}{T_{11} + z_0 T_{12}} \end{cases}, \quad (7)$$

with $z_0 = S/Z_0$. The power dissipated by the ABH then reads $\eta = 1 - |r|^2 - |t|^2 = \alpha - \tau$ with α the absorption coefficient and τ the transmission coefficient. The transmission loss (TL) is defined as $\mathrm{TL(dB)} = -10\log_{10}(\tau)$.

We can take into account the visco-thermal losses within the cavities and the duct using the Johnson-Champoux-Allard-Lafarge (JCAL) model [22], expressed as a function of complex acoustic wavenumbers $k_0' = \omega\sqrt{\rho_{d,c}(\omega) C_{d,c}(\omega)}$ and impedances $Z_0' = \omega\sqrt{\rho_{d,c}(\omega) C_{d,c}^{-1}(\omega)}$ in the transfer matrices of Eq. (6), with $\rho_{d,c}(\omega)$ the effective density that contains the visco-inertial effects and $C_{d,c}(\omega)$ the air compressibility that accounts for the thermal effects. The JCAL parameters have been selected considering the related literature [22].

3. STUDY OF THE INFLUENCE OF THE PHYSICAL PARAMETERS

A comparison has been carried out for validation of the TMM predictions using a Finite Element Method (FEM) commercial programme. ThermoViscous Acoustics model in Comsol Multiphysics considers the gradients of velocity and temperature to include the viscous losses and heat conduction effects. The boundary conditions at the duct sections have been selected to simulate an infinite length duct and avoid plane waves reflected from the inlet and outlet duct sections. The mesh has been defined to warrant at least ten nodal points per acoustic wavelength at the highest frequency of analyses that corresponds to the first duct cut-on frequency $f_c \approx 1.84 c_0/(2\pi R)$. 2D axisymmetric studies have been considered using quadratic elements.

The ABH parameters simulated analytically and numerically correspond to the radius $R = 0.047\,\mathrm{m}$ and the length $L = 0.1\,\mathrm{m}$, that provide a cut-on frequency $f_c = 2142\,\mathrm{Hz}$. The ABH muffler is constituted of $N = 10$ annular cavities of axial width $d = 0.008\,\mathrm{m}$ separated by ring walls of thickness $d_t = 0.002\,\mathrm{m}$, thus leading to a wall porosity $\sigma = d/(d + d_t) = 80\,\%$ over the silencer section. The axial rate at which the cavity depths increase is chosen as $m = 2.4$.

Analytical simulations have been performed using these parameters for the estimation of the absorption coefficient and the TL of the ABH structure. The results are presented in Figure 2.

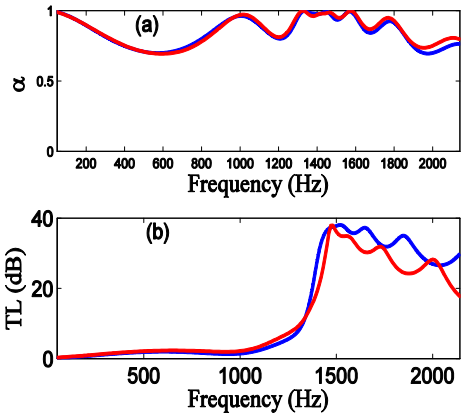

Figure 2. Simulation results for the absorption (a) and the transmission loss (b) for the ABH muffler obtained analytically using TMM (blue) and numerically with FEM (red).

As it can be appreciated, the absorption coefficient presents good performance values over almost the total frequency range of analysis. In particular, in the band between 1300 Hz and 1600 Hz, the absorption exceeds 0.9. In the same frequency range, the corresponding TL exceeds 30 dB. These results show that the proposed muffler acts as an ABH avoiding both reflection and transmission within this frequency range. For low frequencies, the transmission becomes significant and the performance is limited. It can be also seen that the agreement between the analytical and numerical predictions is correct, although for the TL results the FEM underestimates the results provided by the TMM. This could be due to the simplifying TMM approach that discards evanescent interaction between neighboring cavities.

A parametric study has been done to find parametric dependencies and trends for obtaining the maximal dissipation values inside the ABH device. Figure 3 presents the estimated total dissipation $\overline{\eta}$ integrated over a particular frequency band when varying the cavity depth

increase rate m and the length-to-radius ratio L/R. Different frequency ranges between $f_{\min}$ and f_c have been considered for the calculation of the total dissipation $\overline{\eta} = (f_c - f_{\min})^{-1} \int_{f_{\min}}^{f_c} \eta(f) \mathrm{d}f$, which are superimposed in Figure 3. Maximum values are displayed with the corresponding markers.

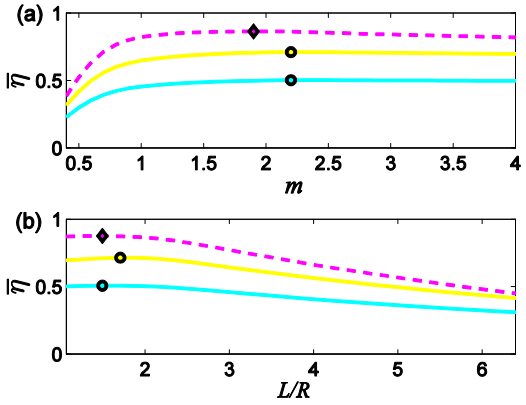

Figure 3. Influence of the cavity depth increase rate m (a) and the length-to-radius ratio L/R (b) for estimating the total dissipated power simulated with TMM and integrated between 100 Hz (cyan), 800 Hz (yellow) and 1200 Hz (pink) up to $f_c = 2142\,\mathrm{Hz}$.

The performance results progressively improve when considered a more reduced frequency range between the lower and the upper frequency limits. When considering the broadest frequency band, the selection of $m = 2.2$ provides optimal dissipation and minimization of reflection and transmission. Concerning the length-to-radius ratio, the value $L/R = 1.5$ can be selected when while keeping a fixed number of cavities $N = 10$. Higher values deteriorate the estimated dissipation progressively. In conclusion, optimal selection of the physical parameters can have an important impact on the expected results. This will be further explored in the next section.

4. OPTIMIZATION BASED ON THE CAUSALITY CRITERION

4.1 Stochastic optimization

Global optimization for the selection of the ABH optimal parameters is a combinatorial optimisation problem where all the physical parameters are cross-related and a variation of one of them may significantly affect the others. The frequency-averaged dissipation over a selected band can also present many sub-optimal maxima and classical optimization algorithms take the risk of being trapped in these non-optimal solutions. Other optimization techniques such as natural algorithms have been used classically. For comparison purposes with the proposed causality-criterion developed in the next section, we have used the Particle Swarm Optimization (PSO), and adaptive optimization techniques that mimic the behavior of certain species group interactions such as birds or fishes. Unlike genetic algorithms, it does not combine genetic materials of previous individuals to progressively improve towards generations, but uses cooperation for the exploration of the search space [23].

We have used a PSO algorithm to find optimal values $(m_{\mathrm{opt}}, \sigma_{\mathrm{opt}}, L_{\mathrm{opt}}, N_{\mathrm{opt}}) = \arg \max_{(m,\sigma,L,N)} \overline{\eta}$ imposing the constraints $0.3 \le m \le 4$, $0.1 \le \sigma \le 0.9$, $1 \le L/R \le 3.4$ and $5 \le N \le 30$ for a given duct radius $R = 0.047\,\mathrm{m}$. The estimation of the averaged dissipation has been done using TMM and the broadest frequency band of interest, from 20 Hz to the first cut-on duct frequency. The optimal values obtained are provided by $m_{\mathrm{opt}} = 2$, $\sigma_{\mathrm{opt}} = 46.7\,\%$, $L_{\mathrm{opt}} = 0.15\,\mathrm{m}$ and $N_{\mathrm{opt}} = 20$. The corresponding optimal cavities width is $d_{\mathrm{opt}} = 0.0035\,\mathrm{m}$.

4.2 Causal-based optimization

A causal-based optimization criterion is formulated in order to find the optimal ABH rings thickness, $d_{t,\mathrm{opt}}$, that maximizes the sensitivity of the total dissipation, integrated over all the positive frequencies, with respect to d_t, i.e. $d_{t,\mathrm{opt}} = \arg\max_{d_t} \left| \partial T_\eta / \partial d_t \right|$ with T_η given by

$$T_\eta = \frac{c_0}{4\pi^2} \left[\int_0^\infty \log[1 - \eta(f)] \frac{\mathrm{d}f}{f^2} \right], \qquad (8)$$

and η calculated by the TMM. This criterion generalizes that already developed for the optimization of rigidly-backed micro-perforated absorbers [7, 8]. Causality implies that η is analytic in the lower half-plane of complex f with no poles, but zeros in this domain if $d_t < d_{t,\mathrm{opt}}$ whereas the zeros are upshifted towards the upper half-plane if $d_t > d_{t,\mathrm{opt}}$. In the former case, the ABH is in under-resistive regime with leakages exceeding the losses

whereas in the latter case, the situation is reversed. When $d_t = d_{t,\mathrm{opt}}$, the losses equate the leakages and the ABH silencer reaches its ultimate wideband performance, but also exhibits a maximum sensitivity to its constitutive parameters, in particular when d_t approaches $d_{t,\mathrm{opt}}$ from the lower values. Examining the variations of T_η with respect to d_t, the other parameters keeping their optimal values found in Sect. 4.1, it is found that the same optimal rings thickness, $d_{t,\mathrm{opt}} = 0.004$ m, already obtained using PSO, is also obtained from the causal-based optimization criterion. According to this criterion, when $d_t = d_{t,\mathrm{opt}}$, the total amount of energy entering the ABH silencer is fully dissipated by visco-thermal losses within the cavities, thereby leading to perfect dissipation above 1.4 kHz up to the duct cut-on frequency.

For the analysis of ABH mufflers, an approach is developed that provides the maximum performance that can be obtained over a target bandwidth with constraints on the muffler geometry. Given that $1-\eta \geq |t|^2$, it results that an upper bound for $T_t = -\left(4\pi^2\right)^{-1}\left[\int_0^\infty f^{-2}\log|t|^2\,\mathrm{d}f\right]$ will also be an upper bound for T_η. Following the same approach presented in [7], one obtains the following inequality

$$T_\eta \leq \frac{c_0}{4\pi}\mathrm{Im}\left[\left.\frac{\mathrm{d}t}{\mathrm{d}f}\right|_{f=0}\right]. \qquad (9)$$

A first-order expansion of $t(f)$ around $f=0$ is found from the TMM formulation. Considering forward transfer matrices between each cell, one gets an explicit expression for $\mathbf{T}_i^{-1}$ from Eq. (6), relating $[p_{i+1},u_{i+1}]^{\mathrm{T}}$ to $[p_i,u_i]^{\mathrm{T}}$. Because the ABH silencer is fully-opened at $z=0$, the transmitted pressure p_{N+1} and volume velocity u_{N+1} are linked by $p_{N+1} = Z_0 u_{N+1}/S$ assuming anechoic downstream condition. One then finds the following causal-based upper bound for the total integrated dissipation

$$T_\eta \leq \frac{L}{4}\left[2+\frac{V_{ABH}}{\sigma V_D}\right], \qquad (10)$$

with V_{ABH} the volume occupied by the ABH and $V_D = SL$ the volume of the lined duct section. Assuming a constant target dissipation η_0 over a specific bandwidth $\Delta\lambda = \lambda_{\max} - \lambda_{\min}$, Eq. (10) provides an upper limit on the ultimate bandwidth-to-length ratio $\Delta\lambda/L$ that can be achieved by the ABH silencer,

$$\frac{\Delta\lambda}{L} \leq \frac{\pi^2}{\left|\log(1-\eta_0)\right|}\left[2+\frac{V_{ABH}}{\sigma V_D}\right]. \qquad (11)$$

Setting $\lambda_{\min} = 0$, a cut-off frequency $f_{\min}$ is deduced from Eq. (11) below which a wideband ABH silencer will exhibit poor dissipation performance. It is given by

$$f_{\min} = \frac{c_0\left|\log(1-\eta_0)\right|}{\pi^2 L\left[2+\frac{V_{ABH}}{\sigma V_D}\right]}. \qquad (12)$$

It follows that decreasing $f_{\min}$ can be achieved by increasing the ABH overall length L or the relative volume V_{ABH}/V_D between the silencer and the duct section or by decreasing the wall porosity σ.

5. EXPERIMENTAL VALIDATION

The performance of the optimized ABH silencer have been verified experimentally in a standing wave facility to measure the reflected, transmitted and dissipated power in plane wave regime. A photograph of the facility is sketched in Figure 4 where the left loudspeaker is connected to the ABH muffler inlet through the impedance tube. It is made of a thick cylindrical tube of length 1000 mm, inner diameter 100mm with its first cutoff frequency at 2.1 kHz. At the end of the tube is plugged a white sample holder in which the ABH muffler can be inserted.

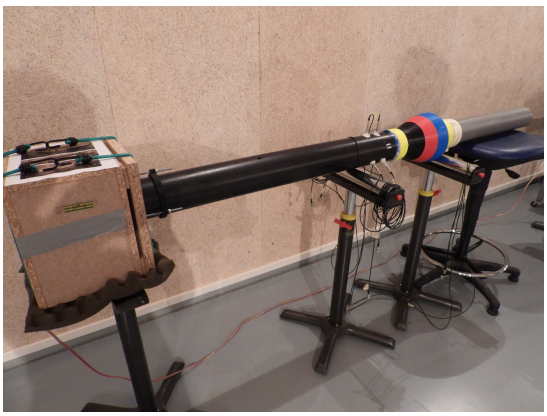

Figure 4. Photograph of the experimental set-up used for the determination of the dissipation of the ABH muffler.

Acoustic characterization is based on the determination of the scattering matrix from the measurements of the transfer

functions between left and right loudspeakers and four flush-mounted condenser microphones separated by a distance $\delta = 5$ cm. The loudspeakers are driven by white noise from 50 Hz to 2.5 kHz. Each acquisition is achieved using the OROS (OR38) multi-channel acquisition system, triggered on the generation of the drive signal, at a sampling rate of 12.8 kHz and with a spectral resolution of 1.56 Hz. It is carried out in the plane wave region between 60 Hz and 2000 Hz with a signal-to-noise ratio (SNR) larger than 10 dB.

An ABH muffler has been fabricated with the optimized parameters using fused deposition modelling of ABS polymer on a heated print surface. The comparison results between the TMM, the numerical FEM and experimental absorption coefficient and TL are presented in Fig. 5.

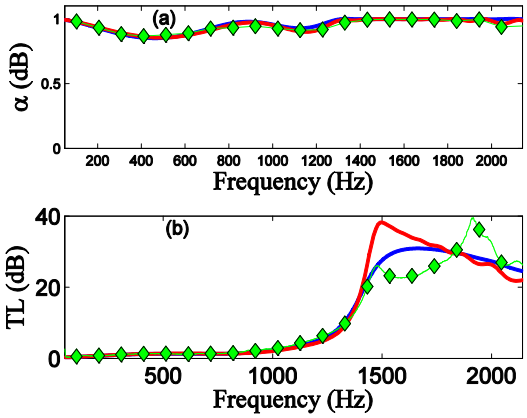

Figure 5. Results for the absorption (a) and the transmission loss (b) for the ABH muffler predicted using TMM (blue), FEM (red) and measured on the experimental set-up (green).

As it can be appreciated, the agreement for the absorption coefficient between the predicted and the measured values is very good. The achieved values are quite remarkable and are maintained almost constant over the whole frequency range of analysis. As for the TL, the estimated and experimental values present more important differences, but it can be noted that the TL values exceed 25 dB above 1400 Hz.

6. CONCLUSIONS

In this work, the concept of sound trapping has been explored for widely-opened ABH silencers aiming at the reduction of the reflection and transmission properties. The study of their performance has been made analytically, using TMM with JCAL model of visco-thermal losses, and numerically, with Visco-thermal Acoustics FEM Comsol Multiphysics. Comparison between the approaches has shown that although TMM overestimates slightly the results provided by FEM due to the simplifying approach that discards evanescent interactions between neighboring cavities, it constitutes a cost-efficient estimation of the ABH performance. It has been shown that the proposed muffler slows down the incident sound wave due to progressive increase of the stiffness-controlled wall admittance. It is able to provide both low reflected and low transmitted powers in the efficiency range that extends between 1300 Hz and 1600 Hz.

Parametric studies using TMM formulation have revealed the impact of the selection of the physical parameters on the acoustic results. In particular, we have shown the influence of the axial rate of increase for the cavity depths and the length-to-radius ratio L/R. A causal-based criterion has been proposed considering the dissipated power integrated over a certain frequency band that can provide an upper bound for the bandwidth-to-length ratio in order to achieve a constant target dissipation. The results have been compared to those obtained from other natural algorithms, such as PSO global optimization and they fit extremely well. Finally, the optimized ABH muffler has been 3D printed with the proposed parameters and the simulated results have been verified experimentally using a standing wave facility to measure the reflected, transmitted and dissipated powers in plane wave regime. The measured results closely follow the predictions within the frequency region of 1300 Hz-2000 Hz, with almost no back-reflected power over this bandwidth.

7. ACKNOWLEDGMENTS

This work is part of the project TED2021-130103B-I00, funded by MCIN/AEI/10.13039/501100011033 and the European Union "NextGenerationEU"/PRTR. It has also received support from the French government under the France 2030 investment plan, as part of the Initiative d'Excellence d'Aix-Marseille Université - A*MIDEX (AMX-19-IET-010).

8. REFERENCES

[1] D. Y. Maa, "Potential of microperforated panel absorbers", Journal of the Acoustical Society of America, vol. 104, pp. 2861–2866, 1999.

[2] D. Y. Maa, "Microperforated-panel wideband absorbers", Noise Control Engineering Journal, vol. 29, pp. 77–84, 1997.

[3] W. H. Tan, R. Haslina, E. A. Lim and H. G. Chuah, "Optimization of micro-perforated sound absorber using Particle Swarm Optimization (PSO)", Materials Science and Engineering, vol. 670, pp. 012046, 2019.

[4] N. N. Kim, "Optimal design of sound absorbing systems with microperforated panels", PhD Thesis, School of Mechanical Engineering, Purdue University, West Lafayette, Indiana, 2016.

[5] M. Toyoda and D. Takahashi, "Sound transmission through a microperforated - panel structure with subdivided air cavities," Journal of the Acoustical Society of America, vol. 124, pp. 3594–3603, 2008.

[6] T. Bravo, C. Maury and C. Pinhède, "Sound absorption and transmission through flexible micro-perforated panels backed by an air layer and a thin plate", Journal of the Acoustical Society of America vol. 131, pp. 3853–3863, 2012.

[7] T. Bravo and C. Maury, "Causally-guided acoustic optimization of rigidly-backed micro-perforated partitions: Theory", Journal of Sound and Vibration, vol. 520, pp. 116634, 2022.

[8] T. Bravo and C. Maury, "Causally-guided acoustic optimization of rigidly-backed micro-perforated partitions: Case studies and experiments", Journal of Sound and Vibration, vol. 523, pp. 116735, 2022.

[9] R. V. Craster and S. Guenneau, Acoustic Metamaterials. Negative Refraction, Imaging, Lensing and Cloaking. Springer Series in Materials Science, 2013.

[10] S. A. Cummer, J. Christensen and A. Alu, "Controlling sound with acoustic metamaterials", Nature Reviews, Article Number 16001, pp. 1–13, 2016.

[11] M. R. Haberman and M. D. Guild, "Acoustic metamaterials", Physics Today, vol. 69, pp. 42–48, 2016.

[12] M. R. Haberman and A. N. Norris, "Introduction to the special issue on acoustic metamaterials", Journal of the Acoustical Society of America, vol. 139, pp. 3239, 2016.

[13] M. Malléjac, P. Sheng, V. Tournat, V. Romero-García, and J.-P. Groby, "Slow-Sound-Based Delay-Line Acoustic Metamaterial", Physical Review Applied, vol. 17, pp. 044035, 2022.

[14] Y. Mi, W. Zhai, L. Cheng, C. Xi and X. Yu, "Wave trapping by acoustic black hole: Simultaneous reduction of sound reflection and transmission", Applied Physics Letters vol. 118, pp. 114101, 2021.

[15] M. A. Miranov and V. V. Pislyakov, "One-Dimensional Acoustic Waves in Retarding Structures with Propagation Velocity Tending to Zero", Acoustical Physics, vol. 48, pp. 347–352, 2002.

[16] F. A. Pelat, F. Gautier, S. C. Conlon and F. Semperlotti, "The acoustic black hole: A review of theory and applications", Journal of Sound and Vibration vol. 476, pp. 115316, 2020.

[17] O. Guasch, P. Sánchez-Martín and D. Ghilardi, "Application of the transfer matrix approximation for wave propagation in a metafluid representing an acoustic black hole duct termination", Applied Mathematical Modelling vol. 77, pp. 1881–1893, 2020.

[18] X. Zhang and L. Cheng. "Broadband and low frequency sound absorption by Sonic black holes with Micro-perforated boundaries", Journal of Sound and Vibration vol. 512, pp. 116401, 2021.

[19] N. Sharma, O. Umnova and A. Moorhouse, "Influence of flare variation on the low frequency sound absorption of mufflers based on the acoustic black hole effect", in: Proceedings of the Institute of Acoustics, Cardiff, U. K., 23 – 24 April 2018.

[20] G. Fusaro, X. Yu, Z. Lu, F. Cui and J. Kang, "A Metawindow with Optimised Acoustic and Ventilation Performance", Applied Science vol. 11, pp. 3168, 2021.

[21] J. He, Z. Zhou, C. Zhang, Y. Zheng, Y. Li, Y. Li, X. Jiang, and D. Ta, "Ultrasparse and omnidirectional acoustic ventilated meta-barrier", Applied Physics Letters vol. 120, pp. 191701, 2022.

[22] J.-F. Allard and N. Atalla, "Propagation of Sound in Porous Media: Modelling Sound Absorbing Materials", Second Edition, John Wiley & Sons Ltd, Chichester, U. K., 2009.

[23] K. Parsopoulos and M. Vrahatis, "Recent approaches to global optimization problems through Particle Swarm Optimization", Natural Computing vol.116, pp. 235–306, 2002.